

The Intertropical Convergence Zone in the South Atlantic and the Equatorial Cold Tongue

SEMYON A. GRODSKY AND JAMES A. CARTON

Department of Meteorology, University of Maryland at College Park, College Park, Maryland

(Manuscript received 30 October 2001, in final form 25 March 2002)

ABSTRACT

Recent observations from the QuikSCAT and Tropical Rainfall Measuring Mission satellites, as well as a longer record of Special Sensor Microwave Imager winds are used to investigate the existence and dynamics of a Southern Hemisphere partner to the intertropical convergence zone in the tropical Atlantic Ocean. The southern intertropical convergence zone extends eastward from the coast of Brazil in the latitude band 10° – 3° S and is associated with seasonal precipitation exceeding 6 cm month^{-1} during peak months over a part of the ocean characterized by high surface salinity. It appears in austral winter when cool equatorial upwelling causes an anomalous northeastward pressure gradient to develop in the planetary boundary layer close to the equator. The result is a zonal band of surface wind convergence that exceeds 10^{-6} s^{-1} , with rainfall stronger than 2 mm day^{-1} , and an associated decrease in ocean surface salinity of 0.2 parts per thousand.

1. Introduction

Rainfall in the tropical Atlantic is organized into several convective zones. North of the equator, the convergence of the winds associated with the meridional Hadley circulation produces a zone of intense convection, which on monthly timescales is organized into the intertropical convergence zone (ITCZ; see, e.g., Hastenrath and Lamb, 1978). Rainfall in the southern subtropics is distinguished by the presence of the South Atlantic convergence zone (SACZ), which extends southeastward from the great continental convective zone of tropical South America and is generated by moisture convergence between the South Atlantic high pressure and the continental thermal low pressure zones. The SACZ reaches maximum intensity in austral summer (here and after the seasons are generally named relative to the Southern Hemisphere) in phase with intensifying continental heating and convection. Between the two there lies a dry zone of general subsidence and surface divergence. Here we present satellite-based observations of a third poorly documented convective zone, whose appearance is closely connected to seasonal changes in SST. This southern intertropical convergence zone (SITCZ) is a feature of the climatological austral winter and is an important source of freshwater to the ocean in an otherwise strongly evaporative band of latitudes.

Zonally elongated atmospheric convective zones are a common feature of tropical climate. The most prominent of these features in the Atlantic and eastern Pacific is the ITCZ. The ITCZ lies at the junction between the northeast and southeast trade wind systems and is indicated by a narrow (a few degrees wide) band of surface wind convergence and a reduction in wind speed. The latitudinal position of the ITCZ in the Atlantic varies from a minimum close to the equator in boreal spring (March–May) in the west to a maximum extension of 10° – 15° N in late boreal summer (August) in the east. The ITCZ is also closely associated with a band of convective clouds and rainfall, which provides a large source of diabatic heat to the troposphere and freshwater to the ocean.

The dynamics controlling the intensity of the trade wind systems in the tropical Atlantic and the ITCZ is a result of complex processes in which continental convection and influences from the other basins play an important part as well as the seasonally and interannually varying SST of the Atlantic Ocean (Enfield and Mayer, 1997; Chiang et al., 2001; Ruiz-Barradas et al., 2000). The northeastward slant of the ITCZ mirrors the appearance of warm ($>28^{\circ}\text{C}$) SSTs that also undergo a meridional migration with season. Year-to-year fluctuations in the meridional gradient of SST in boreal spring give rise to fluctuations in the southernmost position of the ITCZ by several hundred kilometers (Ruiz-Barradas et al. 2000) with severe implications for the climate of the northeastern region of Brazil.

The northward migration of the ITCZ in late northern spring causes a northward shift of the Ekman down-

Corresponding author address: Dr. Semyon Grodsky, Department of Meteorology, University of Maryland at College Park, 3419 Computer and Space Sciences Bldg., College Park, MD 20742-2465.
E-mail: senya@atmos.umd.edu

welling zone south of the ITCZ as well as the strong Ekman upwelling zone to the north. These changes produce a trough–ridge structure in the oceanic thermocline and a geostrophically balanced eastward North Equatorial Countercurrent. Seasonal changes in surface wind speed and cloud cover, in turn, give rise to strong seasonal variations in surface latent heat release and net solar heating, which are important terms in the heat balance of the oceanic mixed layer in the tropical Atlantic (Carton and Zhou 1997). Freshwater flux can potentially influence the subduction of warm tropical waters as well.

Although less prominent than the ITCZ, the eastern tropical Pacific has a second convective zone, the SITCZ lying south of the equator in the band of latitudes between 10° and 3° S (Kornfield et al. 1967; Hubert et al. 1969). This second convective zone is strongly seasonal, appearing only in austral autumn (March–May) in the longitudinal sector east of 140° W. Recently Lietzke et al. (2001) and Halpern and Hung (2001) have examined the links between the seasonal change in SST and the appearance of the SITCZ. Halpern and Hung (2001) have shown that the development of gradients in SST associated with the presence of a seasonal tongue of cool SST along the equator and warming of the Southern Hemisphere in austral autumn give rise to the SITCZ through SST-induced meridional wind convergence. Strikingly, the SITCZ does not form in El Niño years when the cold tongue is absent (Zheng et al. 1997; Lietzke et al., 2001).

Much less is known about convection in the southern Tropics in the Atlantic sector. The earliest indication of an Atlantic SITCZ appears to have been in a report by Belevich et al. (1976), describing results from the Soviet TROPEX-74 research program. Wind convergence and convection, which appears to be associated with an SITCZ is also evident in the July–August climatology of Hastenrath and Lamb (1978, see their Fig. 1d) based on ship reports. Interestingly, a later analysis of the July–August bimonthly surface wind and outgoing longwave radiation (OLR) by Aceituno (1988, see his Fig. 4) did not show this feature.

In this study we exploit the recent availability of an array of satellite-based products to describe the kinematics of the SITCZ in the Atlantic and to explore its connection to the development of strong SST gradients along the equator during austral winter.

2. Data

This study is based on an analysis of meteorological (wind stress, rainfall, and surface air pressure) and oceanic variables (SST and sea surface salinity). We emphasize remotely sensed observations because of their good data coverage over the oceans. We will focus on the 4-yr period 1998–2001 with multiple satellites.

Three satellite-based surface wind analyses are used in this study. The primary wind dataset is the data from

the SeaWinds scatterometer aboard the QuikSCAT satellite (Graf et al. 1998). The QuikSCAT radar has a continuous 1800-km swath and covers 93% of the ocean each day. The wind estimates have an accuracy of 2 m s^{-1} in speed and 17° – 20° in direction (winds in this area have typical speeds of 5 – 10 m s^{-1}). The data were obtained from the QuikSCAT Web site at the National Aeronautics and Space Administration (NASA) Jet Propulsion Laboratory (JPL) where it is available optimally interpolated onto a regular $0.5^{\circ} \times 0.5^{\circ}$, 12-h grid as described by Polito et al. (2000). The QuikSCAT winds are available from mid-July 1999 until the end of our observation period in September 2001. The longer Special Sensor Microwave Imager (SSM/I) monthly wind velocity record of Atlas et al. (1996) is available for the 13-yr period, 1988–2000, but only on a coarser $1^{\circ} \times 1^{\circ}$ grid. Wind direction for the SSM/I velocity is provided by the European Centre for Medium-Range Weather Forecasts (ECMWF) analysis product. The monthly scatterometer wind velocity of Bentamy et al. (2001) from the first and second European Remote Sensing satellites (*ERS-1/2*) is available during the 9-yr period 1992–2000 on a $1^{\circ} \times 1^{\circ}$ grid.

Our rainfall dataset is based on a combination of measurements from the Tropical Rainfall Measuring Mission (TRMM) Microwave Imager and the Precipitation Radar aboard the U.S.–Japanese TRMM satellite (see Kummerow et al., 2000, and references therein). The data used in this study are the TRMM 3G68 daily combination rainfall products, which are available on a $0.5^{\circ} \times 0.5^{\circ}$ grid from late 1997 to 2001. Recent estimates of Bell et al. (2001) have shown that the accuracy of the TRMM rainfall retrievals depends on rainfall rate and is 35% and 30% at 2 and 4 mm day^{-1} , respectively. For additional comparisons the SSM/I-derived rain rate is used (Wentz 1997; Wentz and Spencer 1998).

For mean sea level atmospheric pressure we rely on the National Centers for Environmental Prediction–National Center for Atmospheric Research (NCEP–NCAR) daily reanalyses of Kalnay et al. (1996), available on a $2.5^{\circ} \times 2.5^{\circ}$ grid. Because of the limited number of direct observations over the oceans we can anticipate that surface air pressure estimates will be noisy. For wind velocity and precipitation we also used the climatology provided by Da Silva et al. (1994) based on the Comprehensive Ocean–Atmosphere Data Set (COADS). The SST used in this study is the NCEP SST analysis based on a combination of in situ SST observations and satellite infrared radiances (Reynolds and Smith 1994). Finally, in order to examine the impact of precipitation on the upper layers of the ocean we examine the historical sea surface salinity data of Dessier and Donguy (1994) in comparison with historical ship drift surface currents provided by the National Oceanic and Atmospheric Administration’s National Oceanographic Data Center (NOAA/NODC; NODC 1995). The surface salinity data have been collected by several means, including engine intake salinometers and bucket mea-

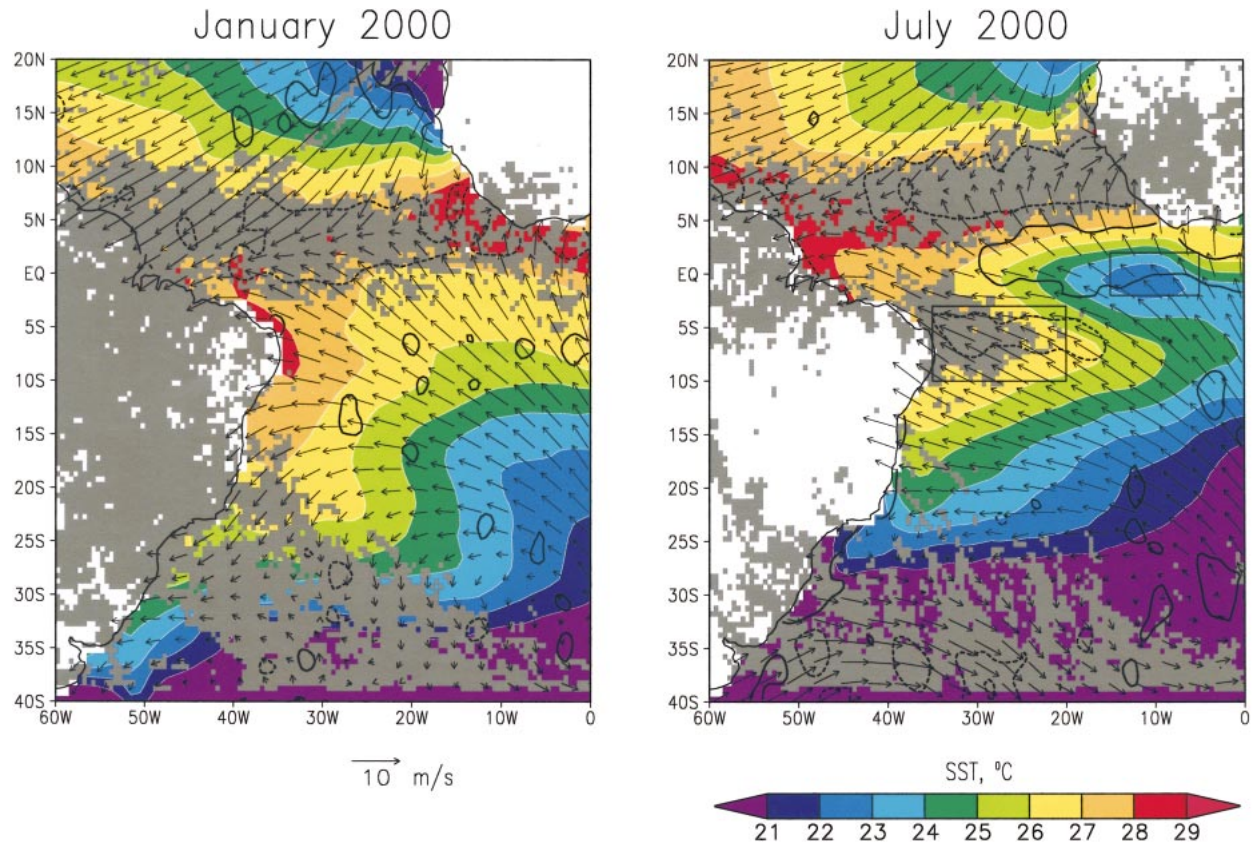


FIG. 1. Monthly average SST (colors), winds (vectors), and rainfall exceeding 2 mm day^{-1} (gray) for Jan and Jul 2000. Wind divergence is contoured at two levels, -5×10^{-6} and $5 \times 10^{-6} \text{ s}^{-1}$, with dashed and solid lines, respectively. The SITCZ index region (10° – 3° S, 35° – 20° W) and the cold tongue region (2° S– 2° N, 15° – 5° W) are indicated by rectangles.

surements. Because of data coverage limitations, we combine observations from many years in order to construct a meaningful seasonal climatology.

3. Results

We begin by considering conditions during the austral summer and winter of the year 2000. In January high SSTs exceeding 28°C occur close to the equator, extending into the Gulf of Guinea and in the west between 10° S and the equator (Fig. 1, January panel). Six months later these high SSTs have shifted northward, while along the equator a tongue of low SSTs ($<24^{\circ}\text{C}$) develops in the longitude band 20°W – 0° . The shift in SSTs from January to July is reflected in a shift of winds and convection. During January the ITCZ is displaced southward over the warm equatorial water in the west with intense convection over the continent of South America and the western half of the basin. The SACZ is evident in the southern subtropics extending southeastward from South America.

By July the ITCZ shifts northward, with increased convection in the eastern half of the basin and reduced convection over the South American continent (Fig. 1, July panel). The SACZ is reduced in strength, while the

SITCZ is visible extending eastward from Brazil in the band of latitudes 10° – 3° S. It is evident that much of the SITCZ convection is confined to the domain 10° – 3° S, 35° – 20° W. We will thus use this region for the purpose of constructing SITCZ indices of rainfall, wind divergence, etc.

The monthly evolution of precipitation, wind convergence, and SST during April–September 2000 is presented in Fig. 2. Beginning in April, wind convergence and precipitation extend south of the equator. During spring this convection is actually part of the ITCZ cloud complex. By June–August the southern branch of the convection separates from the ITCZ and forms the SITCZ, while the ITCZ moves well north of the equator. Surface wind convergence in the SITCZ index region is maximum in July during which time it extends eastward from 35° to 15° W, with values exceeding $5 \times 10^{-6} \text{ s}^{-1}$. This rate of convergence is comparable to that found associated with the ITCZ to the north and, like the ITCZ, is mainly ($>90\%$) associated with meridional, rather than zonal, convergence. The SITCZ produces precipitation east of northeast Brazil peaking at 20 mm day^{-1} (average of 4 mm day^{-1}) in June–July with an accumulated precipitation in the SITCZ index region of 26 cm during June–August 2000. In contrast, climato-

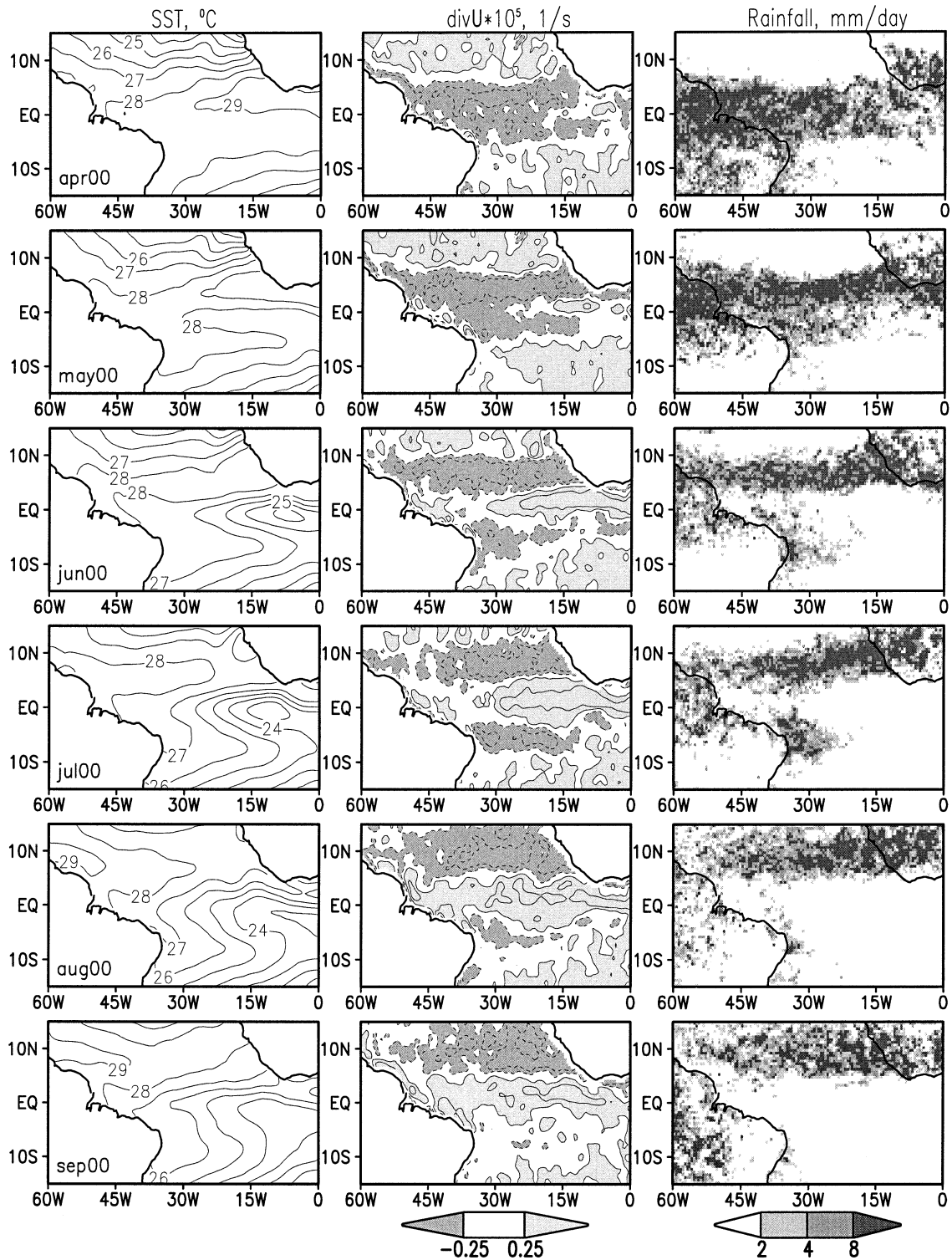


FIG. 2. SST, wind divergence, and rainfall (mm day^{-1}) over the tropical Atlantic during Apr–Sep 2000. Wind divergence and convergence are shown with solid and dashed lines, respectively, starting from $2.5 \times 10^{-6} \text{ s}^{-1}$ with a $5 \times 10^{-6} \text{ s}^{-1}$ contour interval.

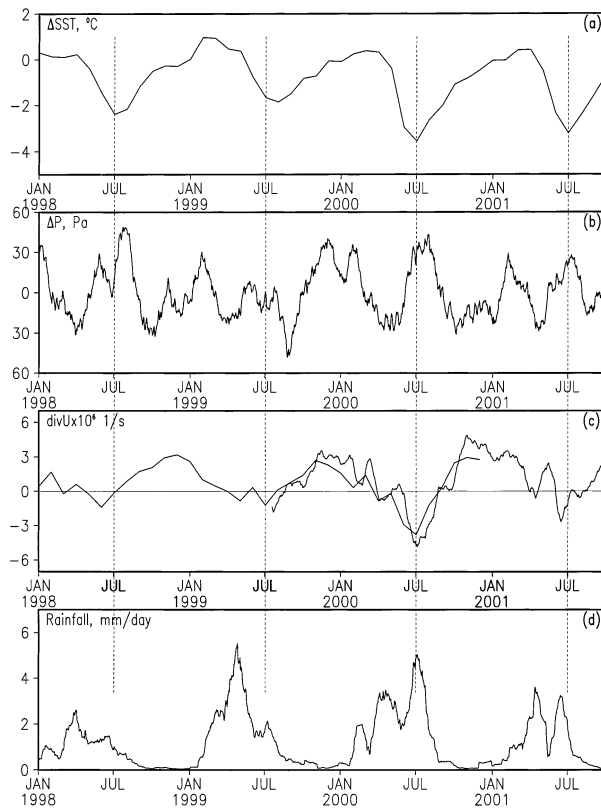


FIG. 3. Monthly averaged meteorological and oceanic time series for 1998–2001. (a) Difference in SST, ΔSST , between the cold tongue and the SITCZ regions; (b) difference in daily sea level pressure, ΔP , between the two regions (after subtraction of a 1-yr moving mean); (c) surface wind divergence, $\text{div}U$, in the SITCZ index region. Two datasets are shown, SSM/I-based monthly winds (1998–2000) and QuikSCAT daily winds (1999–2001). (d) Daily TRMM rainfall in the SITCZ index region. All daily data has been smoothed by a moving monthly average.

logical evaporation in this region during these three months is ~ 45 cm (Hastenrath and Lamb 1978).

The seasonal appearance of rainfall in austral autumn and then again in winter is evident in the time series presented in Fig. 3d that span the TRMM data period, 1998–2001. The autumn maximum, which is associated with the southernmost extent of the ITCZ, is strongest in 1999 when it reaches a maximum precipitation rate of 6 mm day^{-1} (after averaging by a monthly moving filter). In contrast, in the previous year the April–May rainfall barely exceeded 2 mm day^{-1} . The change in the ITCZ position from 1998 to 1999 is closely linked to a cooling of SST north of the equator leading to a reduction in the SST difference between the hemispheres of 2° – 3°C [see Servain (1991) and Ruiz-Barradas et al. (2000) for discussions of the statistical relationships among variables].

In contrast to the April–May precipitation, the June–July precipitation appears most closely linked to the seasonal change in the east-to-west SST difference between the cold tongue region (2°S – 2°N , 15° – 5°W) and

the SITCZ index region, shown in Fig. 3a. This difference in SST, ΔSST , reaches its most negative, generally exceeding 2°C in austral winter, when the cold tongue appears in the eastern basin. The development of a large negative ΔSST coincides with the development of surface wind convergence and an increase in the pressure difference anomaly between the same two regions (Fig. 3b). The pressure difference anomaly, although noisy, varies semiannually with maxima occurring in January and July. We believe that the July maximum in the pressure difference anomaly is the boundary layer response to the development of a zonal gradient of SST along the equator. The austral winter precipitation also varies from year to year, reaching its maximum in 2000, when it exceeds 6 mm day^{-1} , but is less than 2 mm day^{-1} in both 1998 and 1999. Likewise, surface wind convergence exceeds $5 \times 10^{-6} \text{ s}^{-1}$ in 2000, but is less than half that value in the preceding two winters. During these winters the cold tongue was warmer than usual, reducing the magnitude of ΔSST to below $|2^{\circ}\text{C}|$.

Analysis of the longer records provided by the SSM/I satellites and the COADS wind and precipitation datasets confirms that the SITCZ is distinguishable as a feature of climatological July conditions (see Fig. 4). COADS and TRMM rainfall averaged over the SITCZ index region (see inlay to Fig. 4d) has two seasonal peaks. During austral fall rainfall increases due to the southern shift of the ITCZ. During June–July rainfall increases due to the development of the SITCZ.

In order to explore the relationship between ΔSST and wind convergence we examine the relationship between year-to-year changes in both using the 13-yr-long SSM/I dataset complimented by the QuikSCAT monthly averaged winds for the year 2001 (Fig. 5a). For most years (10 of 14) we find a roughly linear relationship. However, during four years 1990, 1992–93, and 1997 wind convergence was absent or weak. Interestingly, two of these years, 1992 and 1997, are El Niño years, suggesting the importance of extrabasin influences. Note also that Pan et al. (2001) found an increase of wind divergence over and around the SITCZ region in the Atlantic in their global spatial EOF of the El Niño mode of wind variation during the El Niño years.

We further investigate spatial patterns corresponding to the wind convergence– ΔSST relationship found in Fig. 5a by projecting the ΔSST anomaly time series on the anomaly of different atmospheric parameters. Anomaly is defined here as a deviation from the mean annual cycle. The projection of the ΔSST anomaly time series on the wind divergence anomaly (computed during austral winter months) shows a stronger wind convergence in the SITCZ index region in response to a cooling of the cold tongue (Figs. 5b,d). The wind divergence anomaly is positive and increases over the cold waters along the equator. The projection of the rainfall anomaly onto the ΔSST anomaly time series shows results consistent with increasing wind convergence around the SITCZ index region that produces stronger

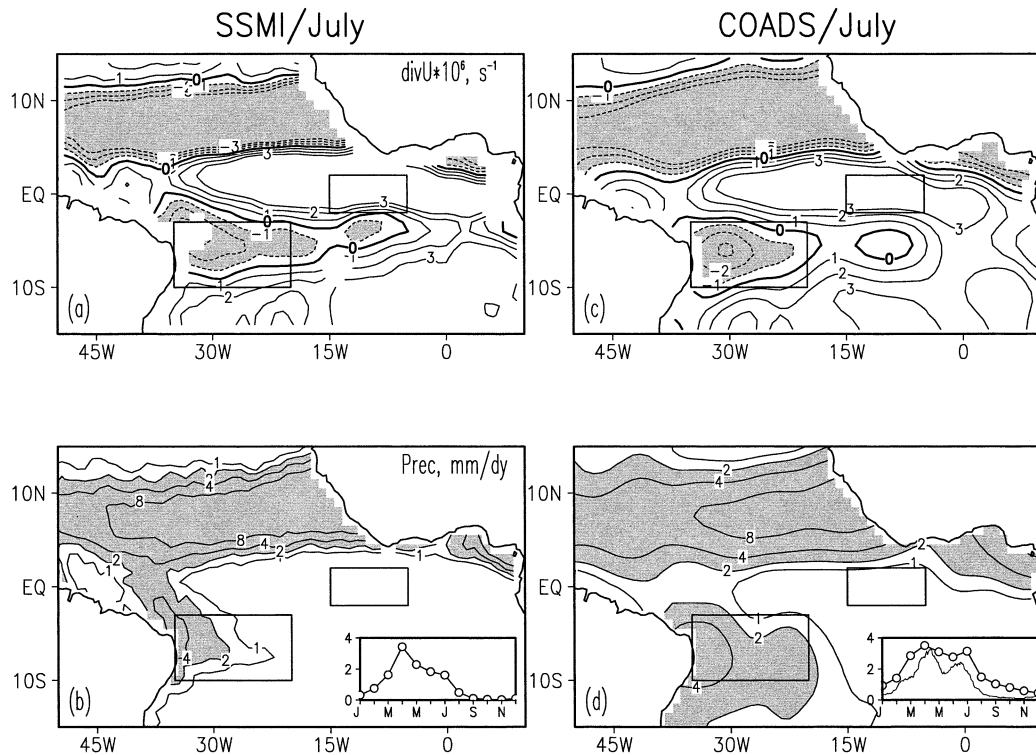


FIG. 4. (a),(c) Jul near-surface wind divergence and (b),(d) precipitation from SSM/I and COADS. The boxes show the SITCZ and the cold tongue index regions. The inlaid plots in (b) and (d) present climatological rainfall averaged over the SITCZ area. TRMM rainfall is also shown in (d).

convection and rainfall there (Figs. 5c). The sea level pressure response is mostly zonal eastward gradient (see Fig. 5e) resulting in an approximately 15-Pa positive pressure difference between the cold tongue and SITCZ areas in response to a negative 1°C year-to-year change in ΔSST .

In order to explore the dynamical relationship between atmospheric and oceanic variables we now introduce a greatly simplified model of boundary layer physics. Neelin and Held (1987) have argued, following the reasoning of Gill (1980), that in highly convective regions diabatic heating, and thus precipitation, should be related to SST. In this region, south of the ITCZ, examination of reanalysis data by Ruiz-Barradas et al. (2000) suggests the presence of a reasonably strong, shallow, trade wind inversion. Thus, here we explore the response of the simple boundary layer model of Lindzen and Nigam (1987) developed for the dynamically similar eastern equatorial Pacific. This model has been previously applied to the tropical Atlantic by Wagner and Da Silva (1994) and Chiang et al. (2001). The model is invoked here only to explore the hypothesis of the SITCZ development in response to the strong westward SST gradient along the equator. It is not expected that such a simple model will capture the entire complexity of the physics of the tropical Atlantic atmosphere.

We assume a well-mixed boundary layer in which

there is a three-term balance among Coriolis effects, $\mathbf{f} \times \mathbf{U}$; pressure gradient forces, $-\nabla p/\rho$; and linear friction, $\varepsilon_u u$, $\varepsilon_v v$:

$$-fv = -\frac{\partial p}{\rho \partial x} - \varepsilon_u u, \quad fu = -\frac{\partial p}{\rho \partial y} - \varepsilon_v v, \quad (1)$$

$$\nabla p = \alpha \nabla T.$$

Or, solving for the surface wind divergence we find that wind divergence depends on the second spatial derivatives of SST:

$$\text{div} \mathbf{U} = \frac{-\alpha(\varepsilon_u \partial^2 T / \partial x^2 + \varepsilon_v \partial^2 T / \partial y^2)}{\rho(f^2 + \varepsilon_u \varepsilon_v)}. \quad (2)$$

In this equation we allow the friction coefficients in the zonal and meridional directions, ε_u and ε_v , to take on differing values of 10^{-5} and $2 \times 10^{-5} \text{ s}^{-1}$, respectively, based on the analysis of Chiang and Zebiak (2000). The coefficient of proportionality between surface air pressure variations and SST, α , is assumed constant and estimated from data in Fig. 5e as $\alpha = -15 \text{ Pa } ^{\circ}\text{C}^{-1}$.

Model results are shown in Fig. 6 for July when the cold tongue reaches its maximum extent and we expect the strongest SST-induced atmospheric pressure change. We evaluate the model only where it is valid south of the ITCZ. In July the development of the cold tongue (positive SST curvature in meridional direction) has caused intensification of divergence along the equator,

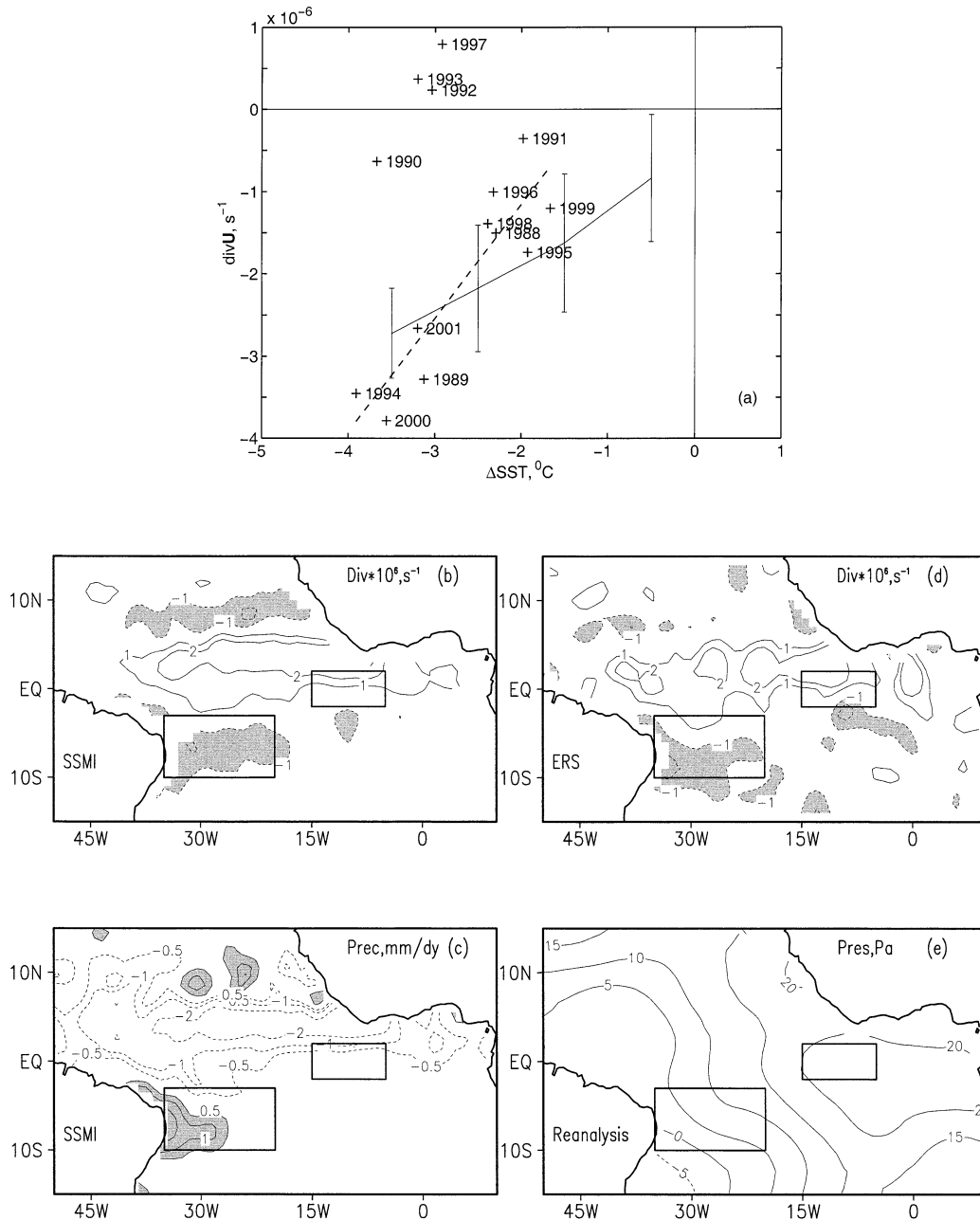


FIG. 5. (a) Jul wind divergence in the SITCZ index region and SST difference between the cold tongue and the SITCZ regions. Dashed line is a linear fit to 10 yr of data excluding 1990, 1992–93, and 1997. Vertical bars are the limits of $\text{div}U$ in the SITCZ index region from the Lindzen and Nigam (1987) model calculated using 20 yr of SST data. The projection of the year-to-year change of the SST difference between the SITCZ and cold tongue regions on the year-to-year change of (b), (d) the near-surface wind divergence, Div ; (c) precipitation, Prec ; and (e) sea level pressure, Pres .

which is also evident to a lesser extent in the observations (see Fig. 4). Six months later (in January, not shown in Fig. 6) the SST gradient is weak and so is the boundary layer response. The strength of the modeled divergence depends on the coefficient relating SST changes to pressure changes. This coefficient should vary with the height of the trade wind inversion, which

we can anticipate should be lower over the cold tongue (Bond, 1992). Allowing α to vary would reduce the summertime divergence. South of the equator between 10° and 3°S, the area of local maximum of SST (negative curvature) produces wind convergence, as observed. The magnitude of wind convergence is consistent with observations (see Figs. 4 and 5a), but the modeled area

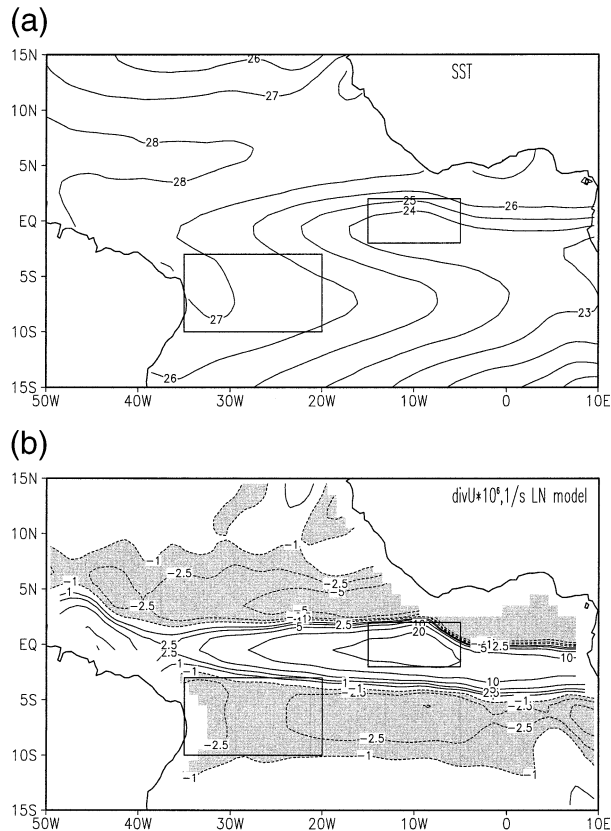


FIG. 6. (a) Jul SST and (b) wind divergence predicted with the Lindzen and Nigam (1987) model.

of convergence extends eastward from Brazil well east of 10°W in contrast to observations. In the convective zone north of the equator the model assumptions are violated and the model produces much less convection than observed.

Next we consider the influence of the SITCZ precipitation on the ocean. If we assume that a precipitation of 4 mm day^{-1} over two months (24-cm total) is distributed over a mixed layer depth of 50 m with an initial salinity (neglecting advective, diffusive, and entrainment processes) of 36 parts per thousand (ppt), then the change in salinity is given by $36 \times (0.24/50) = 0.17$ ppt, approximately corresponding to a significant change in density of 0.15 kg m^{-3} . We explore the possibility of this salinity reduction by examining the historical record of sea surface salinity (SSS) in this region, which fortunately lies within the path of the Europe–Brazil Track #11 of the ship of opportunity program (Dessier and Donguy, 1994).

In Fig. 7a we find that the band of latitudes between 8° and 3°S is characterized by up to a 0.5-ppt local decrease in salinity in July. The 30 cm s^{-1} westward South Equatorial Current (Fig. 7e) in this region is fast enough to flush away the SSS anomalies introduced in April–May. Hence, the SSS anomaly in July is mostly due to July rainfall. Strikingly, the April record of SSS

shown in Fig. 7a demonstrates that the freshening due to April–May rainfall is less pronounced than that due to the June–July rainfall. The time-by-latitude evolution of surface rainfall (Fig. 8) shows that the fresh anomaly south of the equator first appears in spring at 3°S in response to the austral fall rainfall and reaches its lowest values in July at 6°S reflecting the local effect of the SITCZ rainfall (see also Dessier and Donguy, 1994). The 35.8-ppt salinity minimum at 6°S in July (Fig. 8), compared to the surrounding salinity values of 36 ppt, provides an estimate of the surface freshening of 0.2 ppt averaged over the SITCZ index region. This compares well with the calculation of a 0.17-ppt change associated with daily rainfall of 4 mm day^{-1} accumulated during two months.

4. Summary

This paper explores the presence and implications of a southern intertropical convergence zone in the Southern Hemisphere of the tropical Atlantic. Examination of a variety of primarily remotely sensed observations indicates that an SITCZ does appear in austral winter peaking in July–August, a season when the intertropical convergence zone is displaced well to the north. By austral spring the SITCZ is no longer present.

Surface wind convergence during the austral winter of 2000 in the SITCZ index region (10° – 3°S , 35° – 20°W) estimated from QuikSCAT winds was $\sim 5 \times 10^{-6}\text{ s}^{-1}$, a value that is quite comparable to that found in the ITCZ itself. However, the monthly climatological average based on SSM/I and COADS winds gives convergence rates that are lower by a factor of 2. Despite the wind convergence there is little rotation in the surface wind field in the SITCZ region (because as distinct from the ITCZ there is not a calm wind zone), and thus there is only weak Ekman pumping induced in the surface layers of the ocean. During peak months of some years precipitation may exceed 6 mm day^{-1} , but the average precipitation in the SITCZ index region is $\sim 2\text{ mm day}^{-1}$.

We next consider the role of boundary layer processes in producing the observed surface divergence fields. We find that the seasonal appearance of a cold tongue of SST along the equator sets up pressure gradients within the boundary layer that induce wind convergence in the SITCZ index region of the magnitude observed. Indeed, year-to-year changes in the difference in SST between the cold tongue region and the SITCZ index region explain a significant fraction of the year-to-year variability in SITCZ rainfall.

Finally, we examine the oceanic implications of the seasonal SITCZ. We find that there is a seasonal reduction in sea surface salinity of ~ 0.2 ppt (averaged over the SITCZ area) in response to seasonal rains. The southern Tropics have long been identified as a major source of warm water entering the equatorial undercurrent and crossing into the Northern Hemisphere

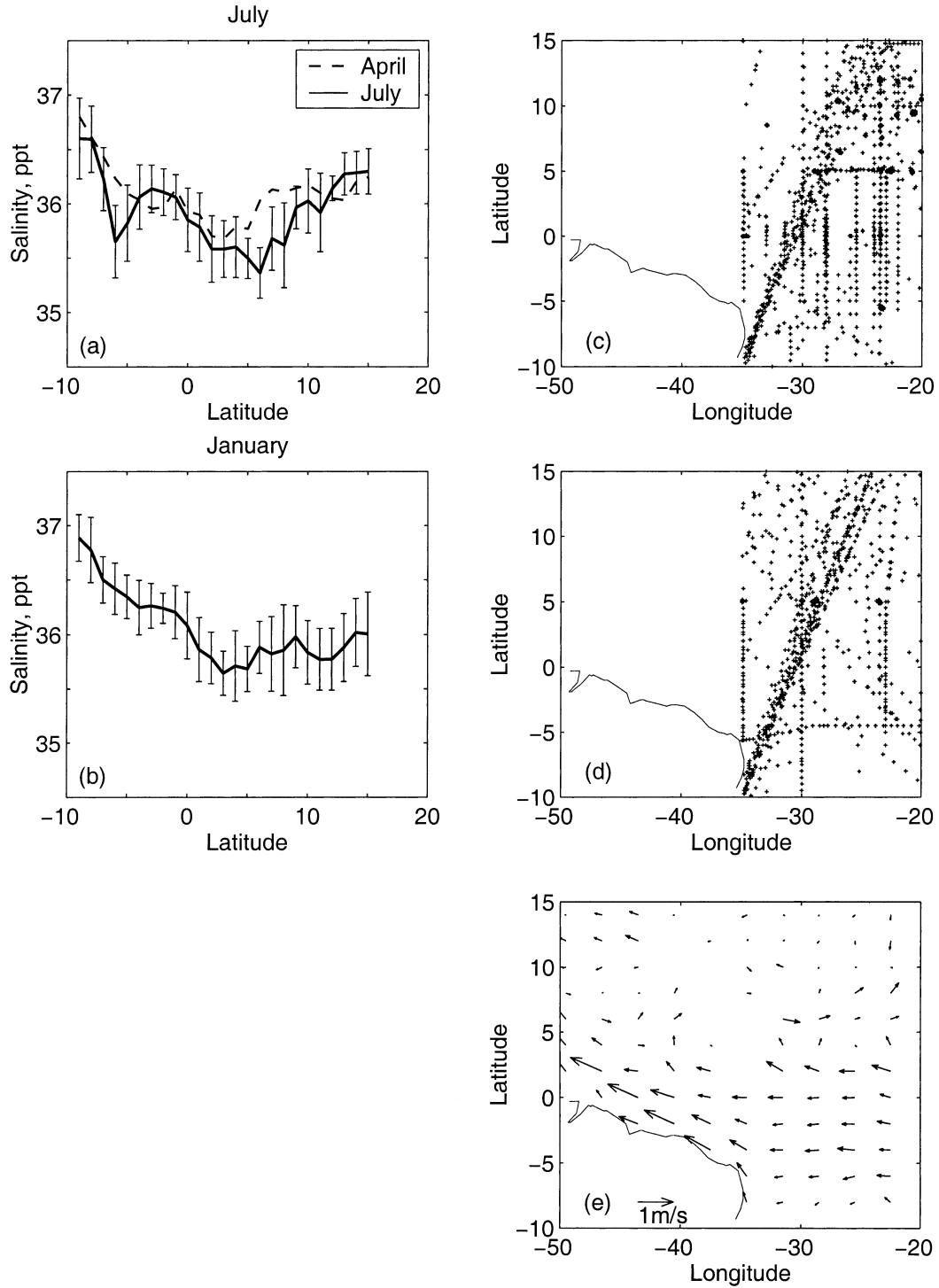


FIG. 7. (a) Jul and (b) Jan sea surface salinity, SSS, averaged between 35° and 20°W vs lat. Vertical bars are std devs of the measurements within 1° lat bands. Locations of observation points between 35° and 20°W for (c) Jul and (d) Jan. (e) Jul surface currents based on historical ship drift.

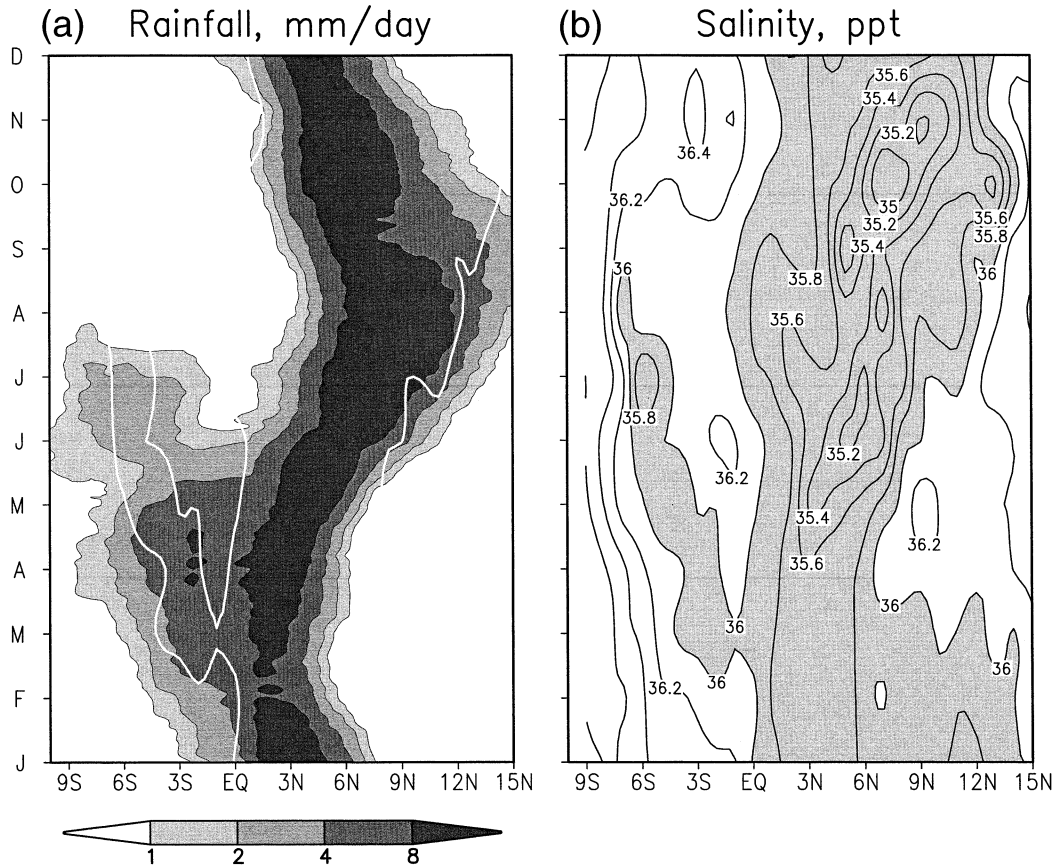


FIG. 8. Latitude–time diagrams of the TRMM seasonal (a) rainfall (mm day^{-1}) and (b) surface salinity (ppt) averaged over 35° – 20° W. Note that the two datasets are not contemporaneous. White line in (a) is 36-ppt salinity contour.

(Metcalf and Stalcup, 1967; Fratantoni et al. 2000), and thus play an important role in climate. Ocean modeling studies will be necessary to exploit this connection.

Acknowledgments. We are grateful to E. Kalnay and S. Nigam of UMD for valuable suggestions. The authors appreciate the support provided by the National Science Foundation (Grants OCE9530220 and OCE9812404). QuikScat wind has been obtained from the NASA–NOAA-sponsored data system Seaflux, at JPL through the courtesy of W. Timothy Liu and W. Tang. A. Dessier kindly provided the sea surface salinity observations. The suggestions given by anonymous reviewers were helpful and stimulating. The gridded TRMM rainfall data are available online at <http://tsdis.gsfc.nasa.gov/trmmopen/3G68.html>. SSM/I wind velocities were kindly provided by R. Atlas and J. Ardizzone. The European Research Satellite-1/2 mean wind field atlas is available online at <http://www.ifremer.fr/cersat>. SSM/I precipitation and water content data are produced by Remote Sensing Systems and sponsored, in part, by NASA's Earth Science Information Partnerships (ESIP): A federation of information sites for earth science; and

by the NOAA–NASA Pathfinder Program for early EOS products; principal investigator: Frank Wentz.

REFERENCES

- Aceituno, P., 1988: On the functioning of the Southern Oscillation in the South-American sector. Part I: Surface climate. *Mon. Wea. Rev.*, **116**, 505–524.
- Atlas, R., R. N. Hoffman, S. C. Bloom, J. C. Jusem, and J. Ardizzone, 1996: A multiyear global surface wind velocity dataset using SSM/I wind observations. *Bull. Amer. Meteor. Soc.*, **77**, 869–882.
- Belevich, R. R., T. S. Demianovskaya, and V. N. Kessel, 1976: On the existence of two intertropical convergence zones in the tropical Atlantic (in Russian). TROPX-74, Leningrad, Russia, Hidrometeoizdat, 736 pp.
- Bell, T. L., P. K. Kundu, and C. D. Kummerow, 2001: Sampling error of SSM/I and TRMM rainfall averages: Comparison with error estimates from surface data and a simple model. *J. Appl. Meteor.*, **40**, 938–954.
- Bentamy, A., P. Flament, Y. Quilfen, and J. F. Piolle, 2001: New release of scatterometer wind field. *Proc. WCRP/SCOR Workshop on Intercomparison and Validation of Ocean–Atmosphere Flux Fields*, WCRP-115, WMO/TD-1083, Potomac, MD, WCRP/SCOR, 233–236.
- Bond, N. A., 1992: Observations of planetary boundary layer structure in the eastern equatorial Pacific. *J. Climate*, **5**, 699–706.

- Carton, J. A., and Z. X. Zhou, 1997: Annual cycle of sea surface temperature in the tropical Atlantic Ocean. *J. Geophys. Res.*, **102**, 27 813–27 824.
- Chiang, J. C. H., and S. E. Zebiak, 2000: Surface wind over tropical oceans: Diagnosis of the momentum balance, and modeling the linear friction coefficient. *J. Climate*, **13**, 1733–1747.
- , —, and M. A. Cane, 2001: Relative roles of elevated heating and surface temperature gradients in driving anomalous surface winds over tropical oceans. *J. Atmos. Sci.*, **58**, 1371–1394.
- Da Silva, A., A. C. Young, and S. Levitus, 1994: *Algorithms and Procedures*. Vol. 1, *Atlas of Surface Marine Data 1994*, NOAA Atlas NESDIS 6, 83 pp.
- Dessier, A., and J. R. Donguy, 1994: The sea surface salinity in the tropical Atlantic between 10°S and 30°N—Seasonal and interannual variations (1977–1989). *Deep-Sea Res.*, **41**, 81–100.
- Enfield, D. B., and D. A. Mayer, 1997: Tropical Atlantic SST variability and its relation to El Niño–Southern Oscillation. *J. Geophys. Res.*, **102**, 929–945.
- Fratantoni, D. M., W. E. Johns, T. L. Townsend, and H. E. Hurlburt, 2000: Low-level circulation and water transport pathways in a model of the tropical Atlantic Ocean. *J. Phys. Oceanogr.*, **30**, 1944–1966.
- Gill, A. E., 1980: Some simple solutions for heat-induced tropical circulation. *Quart. J. Roy. Meteor. Soc.*, **106**, 447–462.
- Graf, J., C. Sasaki, C. Winn, W. T. Liu, W. Tsai, M. Freilich, and D. Long, 1998: NASA Scatterometer Experiment. *Acta Astronaut.*, **43**, 397–407.
- Halpern, D., and C.-W. Hung, 2001: Satellite observations of the southern Pacific intertropical convergence zone during 1993–1998. *J. Geophys. Res.*, **106**, 28 107–28 112.
- Hastenrath, S., and P. Lamb, 1978: On the dynamics and climatology of surface flow over the equatorial oceans. *Tellus*, **30**, 436–448.
- Hubert, L. F., A. F. Krueger, and J. S. Winston, 1969: The double intertropical convergence zone—Fact or fiction. *J. Atmos. Sci.*, **26**, 771–773.
- Kalnay, E., and Coauthors, 1996: The NCEP/NCAR 40-Year Reanalysis Project. *Bull. Amer. Meteor. Soc.*, **77**, 437–471.
- Kornfield, J., A. F. Hasler, K. J. Hanson, and V. E. Suomi, 1967: Photographic cloud climatology from ESSA III and IV computer-produced mosaics. *Bull. Amer. Meteor. Soc.*, **48**, 878–883.
- Kummerow, C., and Coauthors, 2000: The status of the Tropical Rainfall Measuring Mission (TRMM) after two years in orbit. *J. Appl. Meteor.*, **39**, 1965–1982.
- Lietzke, C. E., C. Deser, and T. H. Vonder Haar, 2001: Evolutionary structure of the eastern Pacific double ITCZ based on satellite moisture profile retrievals. *J. Climate*, **14**, 743–751.
- Lindzen, R. S., and S. Nigam, 1987: On the role of sea surface temperature gradients in forcing low-level winds and convergence in the Tropics. *J. Atmos. Sci.*, **44**, 2418–2436.
- Metcalf, W. G., and M. C. Stalcup, 1967: Origin of the Atlantic equatorial undercurrent. *J. Geophys. Res.*, **72**, 4959–4975.
- Neelin, J. D., and I. M. Held, 1987: Modeling tropical convergence based on the moist static energy budget. *Mon. Wea. Rev.*, **115**, 3–12.
- NODC, 1995: *Ocean Current Drifter Data*. National Oceanographic Data Center/National Oceanic and Atmospheric Administration, CD-ROM. [Available online at <http://www.nodc.noaa.gov/General/NODC-cdrom.html>.]
- Pan, J., X.-H. Yan, and W. T. Liu, 2001: Vector empirical orthogonal function modes of the ocean surface wind variability derived from satellite scatterometer data. *Geophys. Res. Lett.*, **28**, 3951–3954.
- Polito, P. S., W. T. Liu, and W. Q. Tang, 2000: Correlation based interpolation of NSCAT wind data. *J. Atmos. Oceanic Technol.*, **17**, 1128–1138.
- Reynolds, R. W., and T. M. Smith, 1994: Improved global sea surface temperature analyses using optimum interpolation. *J. Climate*, **7**, 929–948.
- Ruiz-Barradas, A., J. A. Carton, and S. Nigam, 2000: Structure of interannual-to-decadal climate variability in the tropical Atlantic Ocean. *J. Climate*, **13**, 3285–3297.
- Servain, J., 1991: Simple climatic indices for the tropical Atlantic Ocean and some applications. *J. Geophys. Res.*, **96**, 15 137–15 146.
- Wagner, R. G., and A. M. Da Silva, 1994: Surface conditions associated with anomalous rainfall in the Guinea coastal region. *Int. J. Climatol.*, **14**, 179–199.
- Wentz, F. J., 1997: A well-calibrated ocean algorithm for SSM/I. *J. Geophys. Res.*, **102**, 8703–8718.
- , and R. W. Spencer, 1998: SSM/I rain retrievals within a unified all-weather ocean algorithm. *J. Atmos. Sci.*, **55**, 1613–1627.
- Zheng, Q., X.-H. Yan, W. T. Liu, W. Tang, and D. Kurz, 1997: Seasonal and interannual variability of atmospheric convergence zones in the tropical Pacific observed with *ERS-1* scatterometer. *Geophys. Res. Lett.*, **24**, 261–263.

